ELSEVIER

Journal of Chromatography A, 828 (1998) 121–134

JOURNAL OF CHROMATOGRAPHY A

Adsorption studies of azo dyes as resonance Raman spectroscopic probes at solid–liquid interfaces

Heping Wang[a,*], Patricia M. Callahan[b]

[a]*Brewer Science Inc., 2401 Brewer Drive, Rolla, MO 65401, USA*

[b]*University of Missouri–Rolla, Rolla, MO 65401, USA*

Abstract

The ability to use azo dyes as spectroscopic surface probes has been exploited by using resonance Raman spectroscopy. The experimental results agree well with theoretical considerations in that the ratio of certain Raman scattering bands is linearly related to both pH and the pK_a of indicators, through an empirical relationship which confirmed by theoretical consideration:

$$\log(I_a/I_b) = pK_a + \text{constant} - pH$$

By using azo dye indicators as resonance Raman probes, this method has the unique feature of self-standardization and is applicable to investigate a variety of solid–liquid interfaces. Surface measurement of an HPLC packing material, Separon HEMA Q Bio 1000, shows that there is a substantial indicators' pK_a shift upon indicator adsorption onto this highly charged surface. The shift is caused by electrostatic interaction between anionic dye molecules and the positively charged surfaces of the packing material. Theoretical consideration reveals that the measured shift is proportional to surface potential by:

$$F = 0.059\Delta pK_a$$

With this resonance Raman probe, the surface potential can be computed and the hydrogen ion depletion at the surface can be evaluated. Also discussed are the distance at which the potential is measured based on the ionic strength dependence of the measured potential.

Keywords: Raman spectroscopy; Solid–liquid interfaces; Azo dyes; Dyes

1. Introduction

Solid–liquid interfacial characterization and evaluation are important because they provide information that can reveal the intrinsic aspects of the interfacial interactions between adsorbate and adsorbent. For instance, knowledge of the physico–chemical environment at an electrode surface can lead to an understanding of the electrode process during heterogeneous charge transfer [1]. Another important interfacial example is liquid chromatography in which solute/stationary phase interactions or immobilized ligand/protein interactions are responsible for the retention and selectivity of separations in both HPLC and affinity chromatographies [2–5]. The practical significance of interfacial characterization is that information concerning the surface environment and its effects on solute–stationary phase interactions has led to the development of new column materials for HPLC and affinity chromatography [6,7].

In this study a new HPLC packing material,

*Corresponding author.

0021-9673/98/$ – see front matter
PII: S0021-9673(98)00832-2

Separon HEMA Q Bio 1000, which is an anionic exchanger with a quaternary amino group modified surface, was chosen as the testing material. This strong anionic exchanger has excellent hydrophilic properties and the quaternary ammonium group is not influenced greatly in a mild solvent environment; thus a stable charge is expected to be present on the surface of the beads [8,9].

While maintaining the advantage of allowing a variety of sampling geometries, Raman spectroscopy can provide information about molecular vibrational motion and therefore structural information is available. Thus it is a good choice for interfacial studies. Raman spectroscopy may also be employed with aqueous systems. However, the intrinsic drawback with normal Raman scattering is the very weak scattering signal, especially with monolayer samples. To increase the Raman spectroscopic sensitivity at interfaces, some attempts have been made, i.e. the application of surface enhanced Raman scattering (SERS) [10–12], the utilization of resonance Raman spectroscopy, and the use of more sensitive charge coupled device detectors (CCDs) [13].

In this work, resonance Raman spectroscopy was used to increase the spectroscopic sensitivity. Since the enhanced resonance Raman signal originates from the chromophore which undergoes an electronic transition upon excitation, the spectroscopic information is directly related to the chromophore and its interaction with the environment. To reflect the overall environment, it is desirable that the dye molecule itself be simple and sensitive, of which the chromophore is the major portion. Several authors have used an azo dye, Congo red, to probe ligand–protein interactions [14–17] and have found it to be a valuable conformational probe. Azo dyes contain several aromatic rings which are conjugated with the azo group, thereby making the azo dye molecule more sensitive to the hydrophobicity of the environment [15,18].

The possibility of using azo dyes as resonance Raman probes to characterize solid–liquid interfaces was also investigated. Two azo dyes, methyl orange and ethyl orange, which are pH indicators, were used as resonance Raman spectroscopic probes. The unique feature of these probes is that the same indicator molecule can be used as an internal standard. This remarkable property makes interface measurement and characterization possible. The resonance Raman spectroscopic probes are applied to Separon HEMA Q Bio 1000. The charged surface of these particles is characterized in terms of surface potential and surface acidity. The orientation of the adsorbed indicator molecules on the HPLC adsorbent and their distance from the surface have been approximated from the data. Good agreement between the theoretical consideration and experimental results indicates that this method has the potential to be applied to many solid–liquid interfaces.

2. Experimental

Methyl orange (MO), C.I.13025, (Acid Orange 52) 4-[*p*-(dimethylamino)phenylazo]benzenesolfonic acid, sodium salt, was purchased from Aldrich, Milwaukee, WI, USA. Its formula molecular mass is 327.3, dye content ~95%, with a transition interval: pH 3.2 (red) to pH 4.4 (yellow). Ethyl orange (EO), 4-[*p*-(diethylamino)phenylazo]benzenesolfonic acid, sodium salt, was purchased from Aldrich, Milwaukee, WI. Its formula molecular mass is 333.4, dye content ~90%, with a transition interval: pH 3.0 (red) to pH 4.5 (yellow). All indicators were used without any further purification, and their structures are listed in Fig. 1.

Separon HEMA Bio 1000 Q, 7 μm, 2-hydroxyethyl methacrylate and ethylene dimethacrylate copolymer based-HPLC packing material, with quaternary amino group modified surface and capacity of 0.8–1.2 mmol/gram, was obtained from Tessek, Czech Republic.

An Innova 90 Coherent argon ion laser, 12W (Palo Alto, CA, USA) was used as the excitation radiation source. Typical laser power for the interfacial study was 150 mW at sample and higher power was used for the solution systems. The excitation wavelength was 488 nm unless otherwise indicated. Spex 1403, 0.85 *M* Double-monochromator, Spex Industries, Metuchen, NJ, USA, with a resolution power of 4 cm^{-1}, was used for resonance Raman scattering measurement. A 90° scattering collection geometry was used for sampling throughout all experiments. Raman spectra data processing was supported by DM3000R software. A Model 3210 recording spectrophotometer (Hitachi, Japan) was used for both

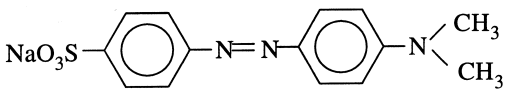

Methyl Orange

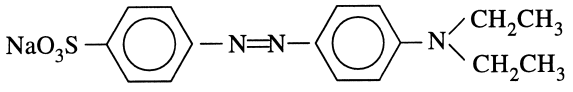

Ethyl Orange

Fig. 1. Structures of azo dyes used in this study.

absorption spectral measurement and quantitative analysis of dyes and proteins.

2.1. Spectrophotometric quantitative analysis of ethyl orange and methyl orange

After dissolution in 0.05 M NaOH, EO absorbance was measured at 472 nm. The linear range spans 0.2–5.0 μg/ml EO under the above conditions. MO absorbance was measured at wavelength of 507 nm in 0.01 *M* HCl solution. The linear range is 0.2–14.0 μg/ml MO under the above conditions.

2.2. Raman sample preparation

25–30 mg HEMA Q adsorbent was washed twice with deionized water in 1.5 ml plastic vial. After centrifugation, the supernatant was discarded, then indicator solution which is buffered with 0.01–0.05 *M* sodium acetate at the desired pH value, was added to make the total volume 1.0 ml. The amount of indicator in the whole system varies in the range 125 μg to 500 μg so that the weight ratio of indicator to HEMA Q adsorbent is within 0.005–0.02. The mixture was allowed to stand 30 min. The sample was centrifuged, the supernatant was discarded, and the slurry was drawn up into a capillary of 1 mm diameter. The capillary was centrifuged to separate the remaining solution. Both ends of the capillary were fused by a flame; the sample was then ready for Raman measurement.

3. Results and discussion

3.1. Theory for resonance Raman probe intensities

An indicator has a certain color transition range; for instance, EO has a range of 3.3 (red)–4.8 (orange), which corresponds to spectroscopic absorption at 507 nm for the acidic color form and 472 nm for the basic form. The vibrational features that accompany the electronic transitions of these two species are very distinctive in their resonance Raman spectra, which allows the use of these Raman features as a qualitative identification of the respective colored species.

In quantitative terms, we can also use the appropriate Raman scattering intensities at the characteristic peak positions to calculate the amounts of each respective colored species. Since the Raman signal is a light scattering response, we can quantify the correlation between the Raman scattering intensity and the appropriate chemical species concentration with the following equations:

$$I_a = \kappa_a[\mathrm{HIn}] \quad (1)$$

and

$$I_b = \kappa_b[\mathrm{In}^-] \quad (2)$$

where I_a and I_b are Raman scattering intensities from the protonated dye molecules (acidic form) and the deprotonated species (basic form), respectively. κ_a and κ_b are constants, which are independent of concentration but are functions of the experimental parameters. [HIn] and [In^-] are analytical concentrations of the indicator molecular acidic form HIn and basic form In^-.

By using the equilibrium condition for the indicator, if it is considered as a conjugate acid–base pair; we get:

$$\mathrm{HIn} = = \mathrm{H}^+ + \mathrm{In}^- \quad (3)$$

$$K_a = [a_{\mathrm{H}^+}][a_{\mathrm{In}^-}]/[a_{\mathrm{HIn}}] \quad (4)$$

or

$$\log\{[a_{In^-}]/[a_{HIn}]\} = \log\{[In^-]/[HIn]\} + \log\{[\gamma_{In^-}/\gamma_{HIn}\} = pH - pK_a \quad (5)$$

where K_a is the dissociation constant of the indicator dye, a_{H^+}, a_{In^-} a_{HIn} are activities for hydrogen ion, basic and acidic forms of dye, and γ_{In^-}, γ_{HIn} are activity coefficients for the basic and acidic forms of the dye, respectively.

Combining Eqs. (1) and (2) we have

$$I_a/I_b = \kappa_a/\kappa_b\{[In^-]/[HIn]\} \quad (6)$$

or

$$\log\{[In^-]/[HIn]\} = \log(\kappa_a/\kappa_b) - \log\{I_a/I_b\} \quad (7)$$

If we assume that the activity coefficient ratio is unity, Eq. (5) can be inserted into Eq. (7), and we have:

$$\log\{I_a/I_b\} = pK_a + \log(\kappa_a/\kappa_b) - pH \quad (8)$$

This is the relationship between the resonance Raman scattering intensity ratio of two appropriate peaks and the medium pH. In Eq. (8), pK_a is an intrinsic property of the dye probe, and $\log(\kappa_a/\kappa_b)$ is a constant because the experimental parameters are exactly the same for both peaks and they cancel each other. The importance of presenting Raman data in this way is that no internal standard is necessary. As a matter of fact, this is essential when dealing with surface adsorption because it is difficult to find an internal standard that adsorbs on the surface with a constant ratio with the azo dye at all pH levels. Eq. (8) shows that the Raman intensity ratio has a linear relationship with respect to the medium pH and that the medium pH can be expressed in terms of Raman intensities. It needs to be pointed here that since Eqs. (1) and (2) are strictly valid only in the ideal case where there is no interference or superimposed peaks at these wavenumbers. As indicated later in the experimental section, however, there are some interference from residual peaks which may cause reduction of linear range. This background interference can be minimized by using empirical construction of relationship stated in Eq. (8).

3.2. Dyes as resonance Raman spectroscopic probes

All dyes in this work have the same chromophore, the azo group –N=N–, and their difference is in their auxochrome groups. Fig. 2 shows the visible absorption spectra at different pH levels for EO and MO. The absorption spectra for both indicators show a shift of maximum absorbance from around 505 nm to 465 nm as the pH decreases. The presence of the isosbestic points for MO at 475 nm and for EO at 510 nm suggests that there are two distinctive chemical species present in the indicator solution system and that there is little or no aggregation present. We interpret these distinct species with maximum absorbance at 505 nm to be the protonated form (acidic form) and the one at 465 nm to be the deprotonated one (basic form).

Corresponding to these absorption changes, or more intrinsically to the electronic state energy changes, the Raman spectra of these indicators at different pH conditions are shown in Fig. 3 and Fig. 4, respectively. Similar Raman spectroscopic features are observed for both compounds because the two indicators have basically the same chromophore. The difference between the auxochrome groups shows some influence on the Raman scattering features in the 1400 cm^{-1} region; these Raman bands correspond to –N=N– stretching vibrations [19,20].

Azo dyes undergo a protonation process in solution with respect to the hydrogen ion concentration change, but the protonation sites have been disputed [21,22]. For instance, the EO molecule has three nitrogen atoms within the molecule, and each of them can be a potential protonation site and thus there are three possible types of protonated dye molecule, as shown in Fig. 5. It is clear that to inquire into the detailed structures of such processes traditional pK_a determination and visible–UV absorption spectroscopy are not adequate. Machida et al. investigated resonance Raman spectra of ^2H and ^{15}N substituted azo dyes and were able to extract information on the structures that the processes involved with color change also correlate with changes induced by pH [23,24]. They suggested an N-ring quinoid type protonation. Type B protonation in Fig. 5 appears only in extremely acidic media. If the acidic form of the probe has a quinoid protonated

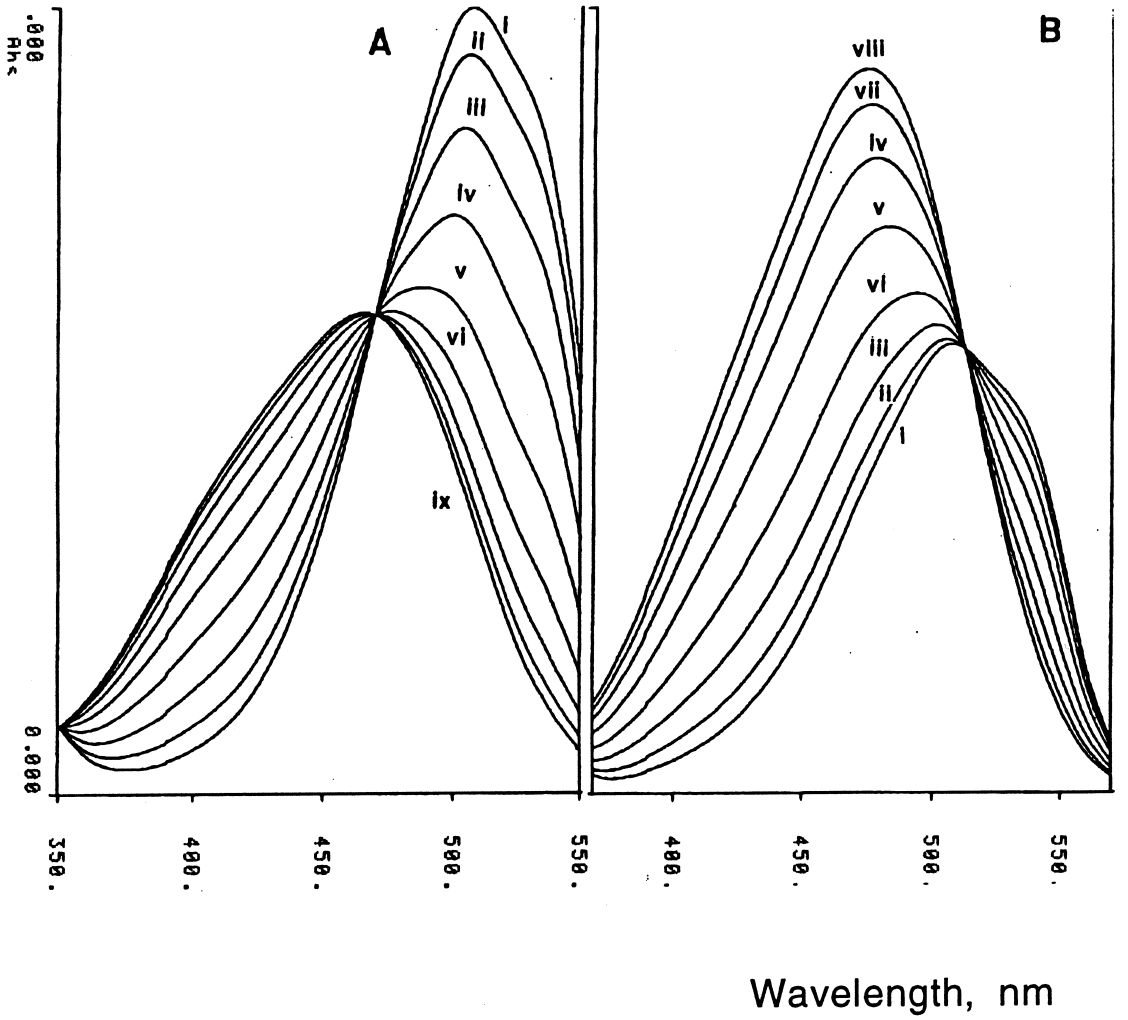

Fig. 2. Absorption spectra of methyl orange and ethyl orange. A: Samples were composed of Methyl Orange, 10 μg/ml, 0.05 *M* sodium acetate. pH at which spectra i–ix were taken: 2.5, 2.8, 3.1, 3.4, 3.7, 4.0, 4.3, 4.6, 4.9. B: Samples were composed of Ethyl Orange, 10 μg/ml, 0.05 M sodium acetate. pH at which spectra i through viii were taken: 3.0, 3.3, 3.6, 3.9, 4.2, 4.5, 4.8, 5.1.

type, it must have the structural characteristics of –C=N– bond and distinctive –C=C– bond other than the substituted aromatic ring, therefore, the Raman spectra should have distinctive features of motion related to these two functional groups. From the MO and EO Raman spectra in Figs. 3 and 4, we do find scattering bands at approximately 1625 cm^{-1} which was assigned by Uno et al. [24] as –C=C– stretching, and a moderately strong band at 1420 cm^{-1} which was assigned as –C=N– stretching. In addition, upon protonation, the azo group in the basic form of the probe is converted to a hydrazone group –HN–N=, thus we find a –N–N– stretching at 1190 cm^{-1}, compared with the basic form –N=N– stretching at 1422 cm^{-1}. A lower frequency agrees well with the bond order change from two to one. The acidic form of the probe is also under resonance condition because the hydrazone group is still in conjugation with both aromatic rings. Raman spectral interpretation in this study is based on the Uno and Machida et al. protonation scheme, i.e. Type A in Fig. 5 [25,26].

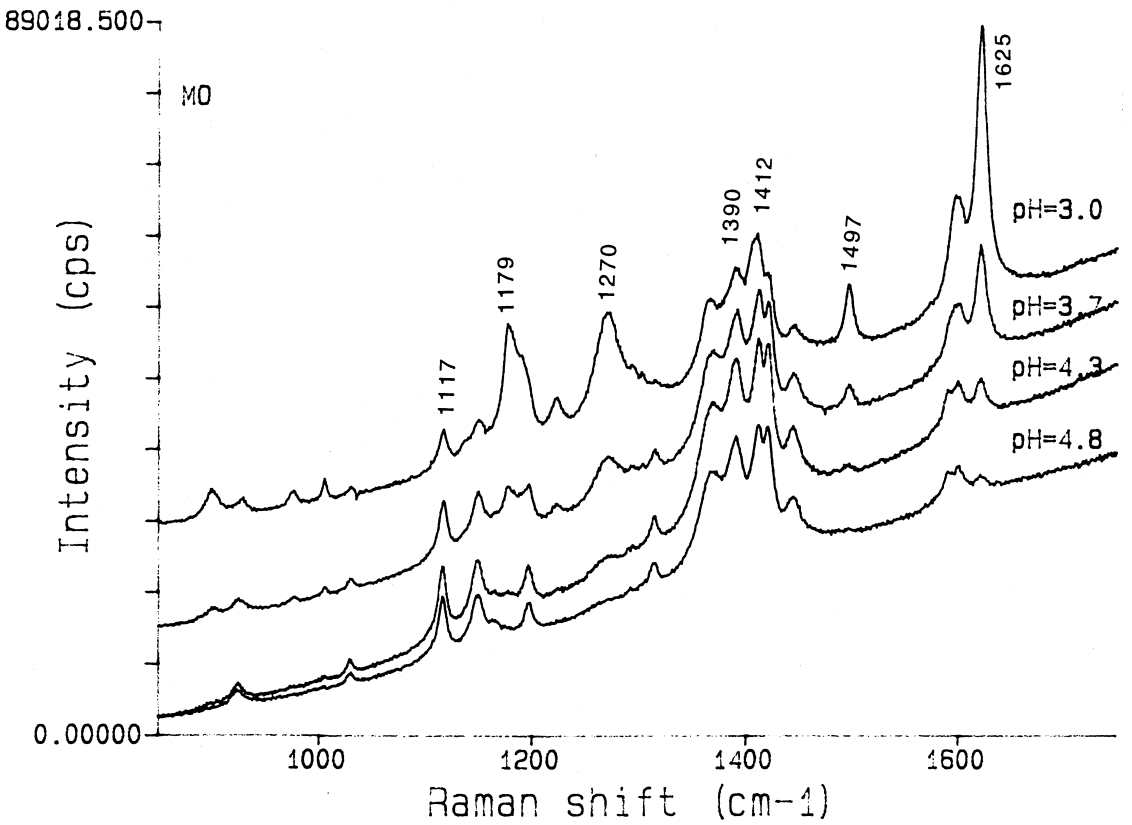

Fig. 3. Raman spectra of methyl orange in solution at different pH levels. MO concentration: 0.05 μg/ml, Laser power at sample: 150 mW, Excitation wavelength: 488 nm.

An important feature of the resonance Raman spectra is that the Raman scattering intensity at 1625 cm^{-1}, resulting from –C=C– stretching, increases with a decrease of solution pH, while the Raman scattering intensity at 1120 cm^{-1}, which was assigned by Cataliotti et al. as C–H in-plane-bending [19] in the deprotonated form, shows the opposite trend with respect to the pH change. This distinctive resonance Raman intensity dependence on solution acidity suggests that these bands can be utilized to represent the respective species concentrations quantitatively. The concentrations of the acidic and basic forms are a function of medium hydrogen ion concentration, as are the Raman scattering intensities which are proportional to the concentration of the appropriate form of the indicator, as demonstrated in Eqs. (1) and (2).

To quantify a species in a solution system, an internal standard is needed to minimize the fluctuation of experimental conditions. The Raman intensity is usually presented as a ratio relative to the internal standard. Sulphate and perchlorate were used for the indicator dye/HEMA Q system and both displayed distinct peaks relative to azo dyes and maintained fairly constant Raman intensity within a reasonable range of acidity; however the sulfate intensity decreased for pH values below 3.5. Even though the perchlorate band intensity was constant to a lower pH level, a constant adsorption ratio of perchlorate with respect to the indicator could not be maintained on the solid surface. Some sort of internal standard is still required for accurate quantification.

As demonstrated in Eq. (8), the Raman scattering intensity ratio of selected peaks is directly proportional to the acidity of the medium. In this study we use the Raman intensity ratio of the band resulting

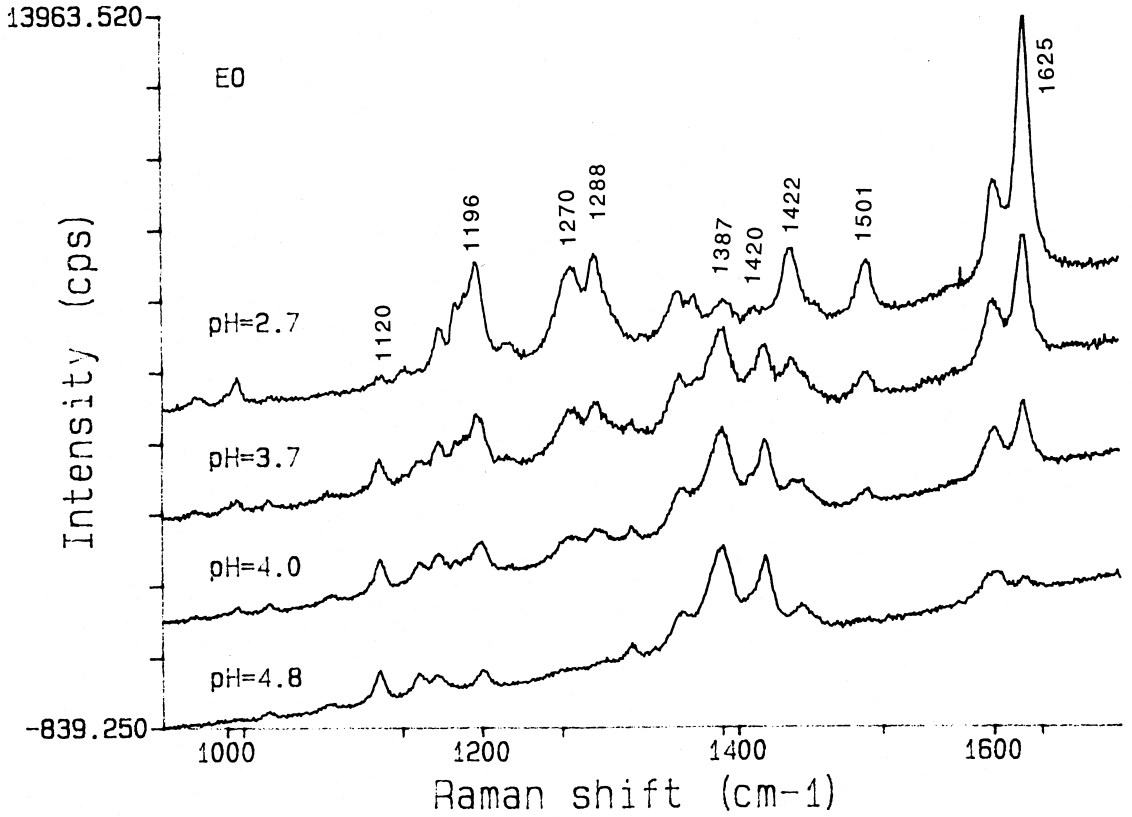

Fig. 4. Raman spectra of ethyl orange in solution at different pH levels. Sample comprised EO: 50 μg/ml, sodium acetate: 0.05 *M* Laser power at sample: 110 mW, Excitation wavelength: 488 nm.

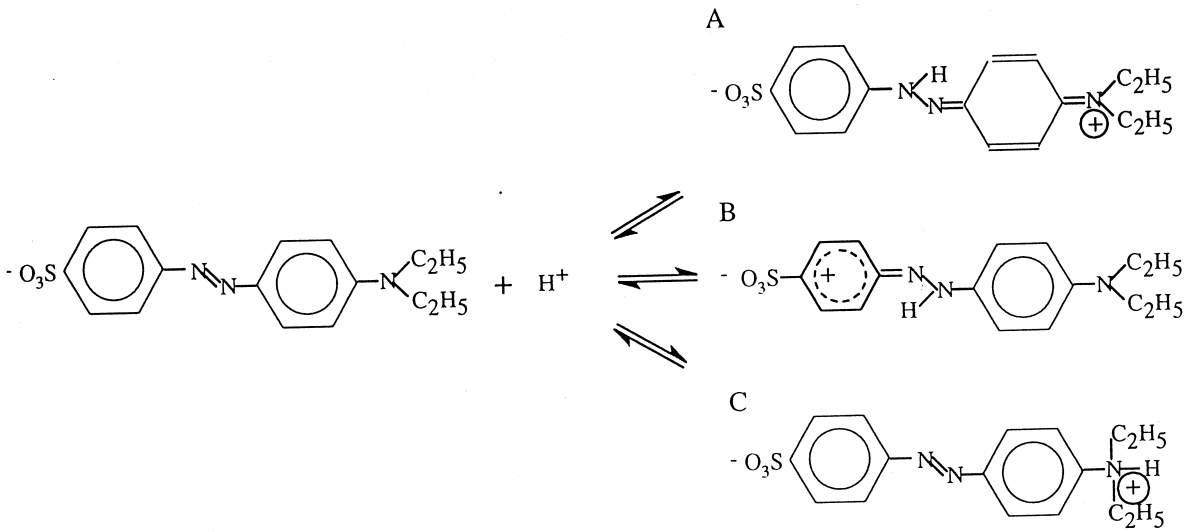

Fig. 5. Ethyl orange protonation scheme in aqueous solution.

from –C=C– stretching in the protonated quinoid N-ring at 1625 cm^{-1}, and that resulting from C–H in-plane-bending in the deprotonated form at 1120 cm^{-1}, to quantify the solution and interfacial environment. When the Raman scattering intensities are represented as such a ratio, any experimental parameter fluctuation will be identical and therefore cancel. In other words, the indicator itself is used as an internal standard and the Raman scattering data are self-standardized. This is an essential requirement for the surface characterization and also an advantage over other quantitative surface methods when dealing with the interfacial adsorption experiments.

The plot of the Raman intensity ratio with respect to the solution pH is shown in Fig. 6. A very good agreement between the experimental results and theoretical consideration has been observed. The small difference between MO and EO may result from the difference of their pK_a values, as a consequence of the small difference in their auxochrome groups.

The significance of this plot is that:

(1) The acidity of a medium can be represented quantitatively in terms of the Raman spectra for a pH sensitive dye. For some situations, where conventional techniques are not applicable, this can be an effective alternative for pH measurement.

(2) For surface characterization, a proper internal standard is usually required to quantitatively determine the surface environment. With the advantage of self-standardized Raman data, this Raman technique can be applied to interfacial systems.

3.3. Azo dye adsorption onto HEMA Q packing materials

Dye adsorption onto HEMA Q was carried out by changing the dye concentration while maintaining the amount of HEMA Q constant. The result is shown in Fig. 7. From the figure it can be seen that there is a very strong affinity between the indicator and the HEMA Q adsorbent. Maximum dye adsorption onto HEMA Q was tested and it showed that over 3.0 mg indicator per 30 mg dry HEMA Q is adsorbed. pH has only a minor effect on the adsorption level at low indicator concentrations, shown in Fig. 8, except at extremely low pH (i.e. pH$<$1.5). For the purpose of the Raman scattering experiment, the desired amount of indicator on HEMA Q ranged from 0.05 mg to 0.2 mg indicator per 30 mg HEMA Q. This amount is far below the maximum capacity of HEMA Q, therefore, no

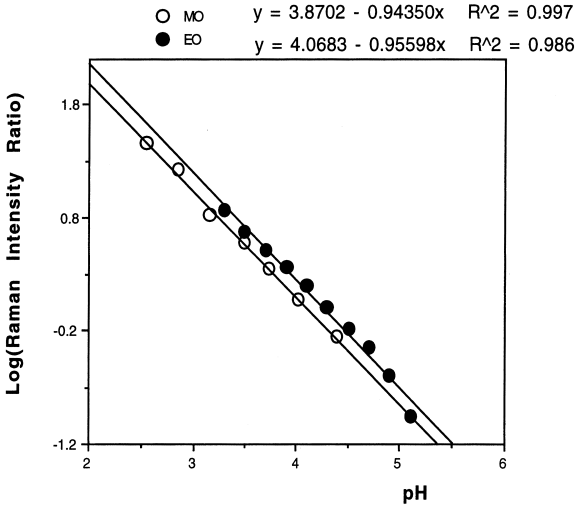

Fig. 6. Plot of the ratio of Raman scattering intensity at appropriate peaks with respect to solution pH. ○=Methyl Orange, $\log(I_{1622}/I_{1117})$. ●=Ethyl Orange, $\log(I_{1624}/I_{1120})$.

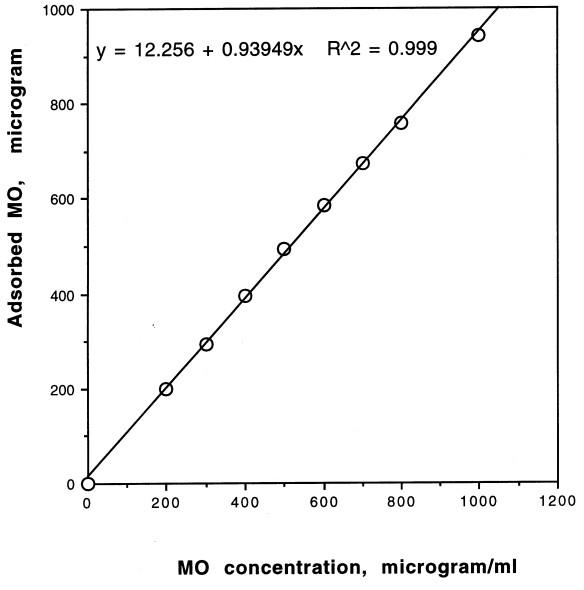

Fig. 7. Methyl orange adsorption isotherm on HEMA Q adsorbent. pH=4.2, HEMA Q mass 30 mg, total volume: 1.0 ml, pH=4.2.

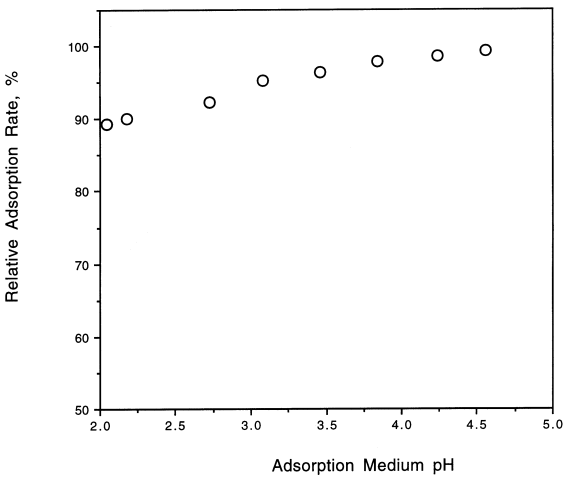

Fig. 8. Effect of adsorption medium pH on relative adsorption level of methyl orange onto HEMA Q. Samples were composed of 0.02 *M* sodium acetate, 20 mg HEMA Q, 0.5 mg MO, in total volume of 1.0 ml.

further tests were conducted to determine the optimal adsorption level.

3.4. Surface characterization of Separon HEMA Q Bio 1000 using resonance Raman scattering of azo dyes

The good agreement between the theoretical prediction and experimental results of dye indicators in solution as a Raman spectroscopic probe of pH has enabled us to extend this technique to surface characterization. Separon HEMA Q Bio 1000, an HPLC packing material was used as the surface support.

With sample cooling, the adsorbed indicator on HEMA Q was subjected to laser Raman measurement and the typical Raman spectra obtained are shown in Fig. 9. From the figure, it is clear that the indicator at the surface also displays similar vi-

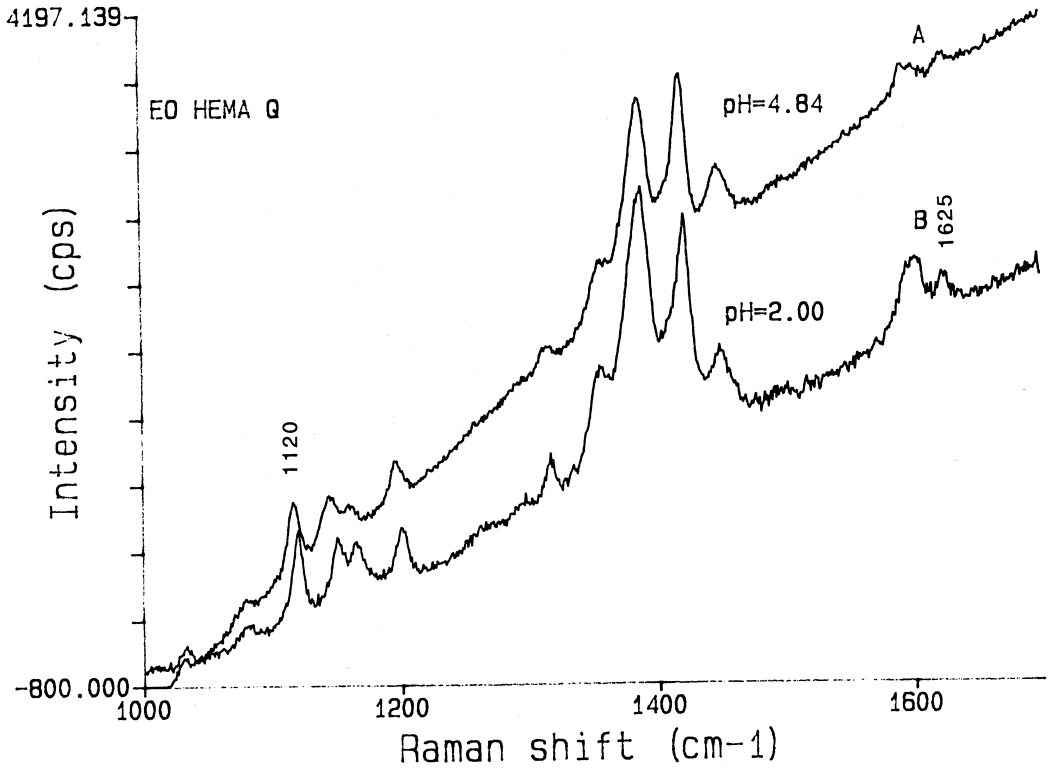

Fig. 9. Raman spectra of adsorbed EO onto HEMA Q and EO in solution. A: Sample was composed of EO: 20 μg/ml, sodium acetate: 0.05 *M*, pH = 4.84, Laser power at sample: 110 mW, B: Sample was composed of 0.3 mg EO adsorbed on 30 mg of HEMA Q in 0.05 *M* sodium acetate, solution pH = 2.00, Laser power at sample: 180 mW. Excitation wavelength: 488 nm.

brational features as those observed in solution. The comparison of the surface Raman scattering spectrum of the adsorbed azo dye with that from solution reveals, at a given pH, that the surface Raman scattering data gives a substantially lower intensity ratio relative to that for the solution system. In other words, although measured at the same pH, the adsorbed dye seems to indicate a higher pH about the surface than in the bulk. To illustrate this quantitatively, a plot similar to Fig. 6 was made for the adsorbed indicator dye, and Fig. 10 displays the data for both the solution state and adsorbed indicators. The straight line equations based on the Raman intensity data show that, although parallel and linear, there is a clear difference of about 3.0 pH units in the intercept of the equations. Based on Eq. (8) and also considering that the hydrogen ion activity at the surface vicinity is the same as in the bulk, this intercept difference can be attributed to a pK_a shift of the azo dye upon adsorption to the HEMA Q surface.

By considering the electric double-layer structure close to the surface, the origin of this intercept difference between the bulk solution and the charged surface can be understood. The positive charges at the HEMA Q will generate an electric field. Any chemical species adsorbed onto a surface will be subjected to an electrostatic interaction within the double layer. The different net charges on both the protonated and deprotonated forms of the indicator will have different interactions with this positively charged electric field. This electric field will repel the like-charged or less-negatively charged species, i.e. the protonated form of indicator, resulting in a surface depletion for such chemical species. Therefore, this electrically selective adsorption will lead to a different equilibrium from that in the bulk solution. This effect is believed to be the origin of pK_a shift at the surface. Some authors have observed the same phenomenon [27,28] and considered the spectroscopic difference as the pH difference between surface and bulk solution [29–31]. However, we disagree with that conclusion based on the fact that the hydrogen activity (as distinct from the hydrogen concentration) throughout the system, including the bulk solution, must be the same [32,33].

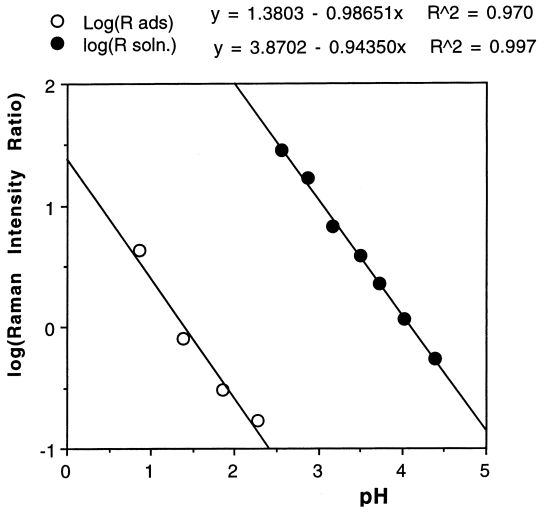

Fig. 10. Comparison of linear plots of Raman intensity ratio versus solution pH for adsorbed EO and EO solution. Experimental conditions are the same as in Fig. 9. ○=Measured in Adsorbed State. ●=Measured in Solution State.

Quantitatively, considering the chemical potentials for both the acidic and basic forms, and for the hydrogen ion in both the bulk solution and in the vicinity of the surface, we assume that the electrical potential is zero in the bulk solution and is Φ at the surface. For the indicator immobilized acidic form, its chemical potential, $\mu_{\mathrm{HIn-s}}$ can be expressed as:

$$\mu_{\mathrm{HIn-s}} = \mu^0_{\mathrm{HIn-s}} + RT \ln [n_{\mathrm{HIn}}/n^0] + RT \ln \gamma_{\mathrm{HIn-s}} - nF\Phi \quad (9)$$

where $\mu^0_{\mathrm{HIn-s}}$ is standard chemical potential for HIn, referring to an uncharged surface, n_{HIn} is the number of acidic indicator molecules adsorbed per unit area of the surface, n^0 is the total number of the surface active sites per unit area, n is the net charge of the indicator in the acidic form, $\gamma_{\mathrm{HIn-s}}$ is the activity coefficient for the acidic form adsorbed onto the surface and, F, and R are the Faraday and gas constants, respectively.

Similarly, for the basic form adsorbed onto the surface, its chemical potential can be expressed as:

$$\mu_{\mathrm{In-s}} = \mu^0_{\mathrm{In-s}} + RT \ln [n_{\mathrm{In-}}/n^0] + RT \ln \gamma_{\mathrm{In-s}} - (n-1)F\Phi \quad (10)$$

where $\mu^0_{\mathrm{In-s}}$ is standard chemical potential for In−, $\gamma_{\mathrm{In-s}}$ is the activity coefficient for the basic indicator immobilized onto the surface.

For the equilibrium expression:

$$HIn_{ads.} \equiv In^{-}_{ads.} + H^{+}_{aq}.$$

we have:

$$\Delta G = \mu_{HIn-s} - \mu_{In-s} - \mu_{H^+}(aq) = 0 \quad (11)$$

or

$$0 = [\mu_{H^+}(aq) + \mu^0_{In-s} - \mu^0_{HIn-s}] + RT \ln [\gamma_{In-s} n_{In} a_{H^+} / \gamma_{HIn-s} n_{HIn}] - F\Phi \quad (12)$$

Since the standard chemical potential for the adsorbed species refers to the uncharged surface, an assumption can be made that

$$[\mu_{H^+}(aq) + \mu^0_{In-s} - \mu^0_{HIn-s}]_{\Phi=0} = (\Delta G^0)_{ads} = (\Delta G^0)_{aq} = -RT \ln K_a$$

then we have:

$$\ln [n_{In-*} a_{H^+} / n_{HIn}] = \ln K_a + F\Phi/RT - \ln [\gamma_{In-s} / \gamma_{HIn-s}] \quad (13)$$

If we define the quantity, $n_{In*8} a_{H^+} / n_{HIn}$ in as an apparent dissociation constant, $K_{a'}$, for the indicator at the surface and make the approximation that $[\gamma_{In-s} / \gamma_{HIn-s}]$ is unity, then we have

$$\ln K'_a = \ln K_a + F\Phi/RT \quad (14)$$

and at standard conditions we will have:

$$\Phi = 0.059 \Delta pK_a \quad (15)$$

where $\Delta pK_a = pK_a - pK'_a$. Eq. (15) indicates the relationship between the pK_a shift and the surface potential, Φ. As shown by the experiment, the quantity ΔpK_a can be readily measured by resonance Raman spectroscopy. This means that by using the Raman scattering spectroscopic method, the electric potential of surface, Φ, can be measured if the azo dye probe can be properly immobilized or adsorbed onto the surface. It is very interesting to notice that if the assumption holds that for an externally applied electric field the pH is the same at the charged surface as in the bulk, and that a proper reference point can be practically defined, we may monitor a single electrode potential without involving another interface.

Since the indicator molecule itself is a charged particle, after adsorption to the surface, the interfacial charge density would be altered. This perturbation of the interfacial potential is not desirable for an accurate surface potential measurement. To evaluate this perturbation effect so as to ensure accurate interfacial potential measurement, the adsorbed amount of indicator was reduced gradually to allow extrapolation of the pK_a shift to zero dye adsorption (the non-perturbation condition). The results are listed in Table 1 for EO, in which surface potentials are calculated according to Eq. (15).

From the table, we can see that no significant potential variation was observed. This implies that a change in the amount of indicator adsorption has little effect on surface charge distribution or neutralization. This could be a consequence of the large loading capacity of the HEMA Q packing material. As a matter of fact, the HEMA Q capacity is as high as 1.2 mmol/gram; 30 mg of support would have adsorbed 13.0 mg of the indicator to its maximum capacity. While in practice, less than 0.15 mg was adsorbed onto HEMA Q, i.e. approximately 1% of its maximum capacity. The portion of the charged sites at the surface that were shielded is quite small compared with the total number of sites. This small

Table 1
Measured ΔpK_a and calculated interfacial potential of HEMA Q with EO as the surface probe

EO, adsorbed (mg)[a]	Bulk pH	ΔpK_a	Potential mean (mV)[b]
0.02	2.49	2.86	183 (2.7%)[c]
	1.93	3.17	
	1.56	3.20	
	1.48	3.20	
0.01	2.62	2.73	172 (0.9%)
	2.00	2.91	
	1.78	2.94	
	1.44	2.90	
0.005	2.04	2.94	171 (0.6%)
	1.47	2.93	
	1.04	2.80	
0.0025	2.27	3.05	180 (2.7%)
	2.01	3.31	
	1.52	2.93	
	1.09	3.01	

[a] Per 30 mg of dry HEMA Q.
[b] Calculated based on Equation: $\Phi = 0.059 * \Delta pH$.
[c] Variance of the Measurement: S/Mean.

amount of adsorbed molecules do not constitute monolayer adsorption, therefore, the shielding effect is insignificant compared with the supporting electrolyte (i.e., typically, 0.05 *M* acetate). Based on the experimental results, it is concluded that when dealing with a highly charged surface, the shielding effect due to probe adsorption is essentially negligible. But for a low charge density surface, the extrapolation method could be applied for accurate surface potential measurement.

From the calculated surface potential data, we can estimate the surface depletion effect for hydrogen ion. Since a positive surface electric field expels like-charged hydrogen ions, the hydrogen ion concentration would be different from that in bulk solution where the electric field is assumed to be zero.

Using the Boltzman distribution law, we have:

$$N_{H^+} = N^0_{H^+} \exp\left[-F\Phi/RT\right]$$

where N_{H^+} is the number of hydrogen ions in the vicinity of the surface and $N^0_{H^+}$ is the number of hydrogen ions in bulk solution, per unit volume, for instance per dm^3. Assuming the electrical potential in the vicinity of surface is 170 mV, at 25°C, the ratio of $N_{H^+}/N^0_{H^+}$ is about $1.27 \cdot 10^{-3}$. This result suggests that, due to electrostatic interaction, the hydrogen ion concentration in the vicinity of the surface is considerably smaller than that in the bulk. This is graphically shown in Fig. 11 in which both surface interface and hydrogen ion concentration distribution profiles are displayed. In the case of HEMA Q, there is a depletion factor of around three orders of magnitude. This information provides certain insight to the solid–liquid interfacial environment in ion-exchange chromatography, because we can have an estimate of the concentration of charged solutes. Similarly, we can also use this technique to estimate the concentration of charged reactants or products within an external electric field, for instance at an electrode surface. Furthermore, if we apply this surface measurement to materials whose surface charge is a function of the bulk solution composition, we can practically measure the point-of-zero-charge (PZC) of those materials. Without specific absorption at the solid–liquid interface, zero charge corresponds to zero surface potential, therefore, when approaching the PZC, based on the Eq. (15), the ΔpK_a between the bulk solution and surface should approach zero. In other words, by determining zero ΔpK_a by using the Raman spectroscopic probe, the PZC of these kinds of materials can be determined.

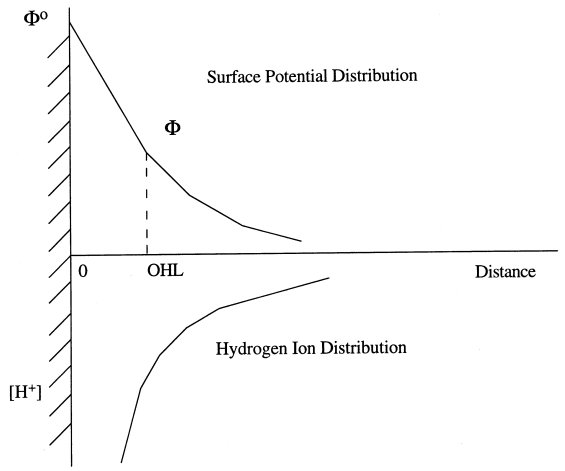

Fig. 11. Graphic presentation of the distribution profile for surface potential and hydrogen ion concentration of charged solid–liquid interface.

The surface potential is greatly influenced by the ionic strength of the bulk system, because the concentration of salt in the medium plays an important role in the construction and alternation of the interfacial double-layer. Based on the Debye–Huckel theory [34,35], we could expect that with an increase of salt concentration, the surface charge would decrease at a fixed distance from the solid surface. This distance is determined by the size and orientation of the surface probe. To investigate this, KCl was used as an ionic strength adjustment salt to understand the ionic effect on the surface potential. The experimental result is shown in Fig. 12, in which the measured surface potential is plotted versus KCl concentration. There is a very good agreement with the expectation, as shown in the figure, in which the surface potential decreases steadily with the increase of KCl concentration. The surface potential decrease, calculated from ΔpK_a based on Eq. (15), results from the suppression of surface potential by high concentration of electrolyte. This dependence of potential on the ionic strength suggests that the indicator may be as close to the surface as the outer Helmhotz layer (OHL) of the interface. The distance

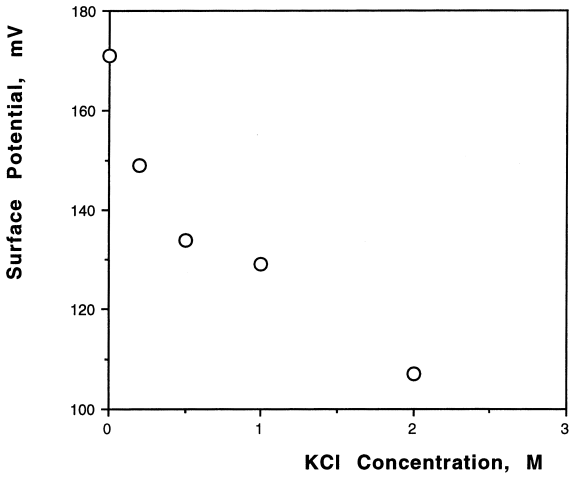

Fig. 12. The effect of ionic strength on solid–liquid surface potential. Samples comprised: HEMA Q: 25 mg, sodium acetate 0.05 *M*, EO 0.2 mg in total volume of 1.0 ml, solution pH = 1.6.

at which the interfacial potential is measured with resonance Raman spectroscopy is determined by the dimension and orientation of the probe.

4. Conclusion

(1) Theoretical consideration reveals that azo dye indicators can be used as resonance Raman probes based on the characteristic Raman scattering of the interconverting species. The capability of dye indicators to be used as probes is expressed in the relationship:

$$\log I_a/I_b = pK_a + \log(\kappa_a/\kappa_b) - pH$$

(2) A good agreement between theoretical and experimental results for ethyl orange and methyl orange, as surface probes, has been observed. This method is applicable to investigate solid–liquid interfaces with the advantage of self-standardized Raman data.

(3) The method was applied to an HPLC packing material, Separon HEMA Q Bio 1000 Surface measurement results show that there is a substantial K_a shift upon indicator adsorption onto this highly charged surface. The K_a shift can be explained by the consideration of selective adsorption of different chemical species which may be caused by the high surface charge of the anionic exchanger.

(4) An attempt has been made to utilize the Raman scattering data to calculate the potential of charged surfaces based on thermodynamic considerations. An equation has been proposed for the relationship between surface potential and K_a shift:

$$\Phi = 0.059\Delta pK_a$$

(5) The distance at which the potential was measured is determined by the dimension and orientation of the probe molecule. The ionic strength dependence of the measured potential suggests that the adsorbed probe molecule may be near the OHL of the charged surface.

(6) Extensions of this method include the measurement of colloidal PZC's and the measurement of external electric field at solid–liquid interfaces, such as electrode surface potential without involving another interface.

Acknowledgements

The authors would like to express their appreciation to Professor G.L. Bertrand of UMR for his direction in thermodynamics in this work and for reading the manuscript. We also would like to thank Dr. I. Vins of Tessek Ltd., Czech Republic, for providing us with the HEMA Q packing material.

References

[1] A.J. Bard, L.R. Faulkner, Electrochemical Methods, Fundamentals and Applications, Wiley, New York, 1980.
[2] M.D. Scawen, Anal. Proc. 28 (1991) 143.
[3] G. Kopperschlaeger, G. Birkenmerier, Affinity Partitioning and Extraction of Proteins, Bioseparation, Klewer, Dordrecht, 1990, p. 235.
[4] M.D. Scawen, J. Darbyshire, M.J. Harvey, T. Atkinson, Biochem. J. 203 (1982) 699.
[5] P. Oroszlan, S. Wicar, G. Teshima, S.-L. Wu, W.S. Hancock, B.L. Karger, Anal. Chem. 64 (1992) 1623.
[6] A. Markauskas, V. Tiknius, R. Marcisauskas, J. Chromatogr. 539 (1991) 525.
[7] S.M. Munoz, M. Caldera, S. Canevari, E. Tosi, T. Cogliati, M.I. Collnaghi, F.P. Conde, Biochem. Biophys. Res. Commun. 173 (1990) 554.

[8] O. Mikes, P. Strop, J. Coupek, L. Rexova-Benkova, D. Chadimova, J. Chromatogr. 257 (1983) 23.
[9] F. Vlacil, I. Vins, J. Chromatogr. 391 (1987) 133.
[10] D. Franzke, A. Wokaun, J. Phys. Chem. 96 (1992) 6377.
[11] H. Yamada, H. Nagata, K. Kishibe, J. Phys. Chem. 90 (1986) 818.
[12] O. Siiman, A. Lepp, J. Phys. Chem. 88 (1985) 2641.
[13] R.A. Matzner, R.C. Bales, J.E. Pemberton, Appl. Spectros. 48 (1994) 1043.
[14] M.M. Federici, E.R. Stadtman, Biochemistry 24 (1985) 661.
[15] R.A. Edwards, R.W. Woody, Biochemistry 18 (1979) 5197.
[16] R.A. Edwards, R.W. Woody, J. Phys. Chem. 87 (1983) 1329.
[17] E. Stellwagen, Acc. Chem. Res. 10 (1977) 92.
[18] R.A. Edwards, R.W. Woody, Biochem. Biophys. Res. Commun. 79 (1977) 470.
[19] R.S. Cataliotti, A. Morresi, G. Paliani, M.Z. Zgiersky, J. Raman Spectros. 20 (1989) 601.
[20] P.R. Carey, H. Schneider, H.J. Berstein, Biochem. Biophys. Res. Commun. 47 (1972) 588.
[21] H. Lee, K. Machida, A. Kuwae, Y. Saito, J. Molec. Struct. 68 (1980) 51.
[22] K. Kumar, P.R. Carey, Can. J. Chem. 55 (1977) 444.
[23] K. Machida, H. Lee, A. Kuwae, J. Raman Spectros. 9 (1980) 198.
[24] T. Uno, B. Kim, Y. Saito, K. Machida, Spectrochim. Acta 32A (1976) 1170.
[25] K.A. Giuliano, Anal. Biochem. 197 (1991) 333.
[26] H. Hacker, Spectrochim. Acta 21 (1965) 1989.
[27] F.M. Mirabella Jr., J. Polymer Sci. 20 (1982) 2309.
[28] O. Wolfbeis, H. Offenbacher, Sens Actuat. 9 (1986) 85.
[29] J. Janata, Anal. Chem. 59 (1987) 1351.
[30] P. Fromherz, B. Masters, Biochim. Biophys. Acta 356 (1974) 270.
[31] K.I. Mullen, D. Wang, L.G. Crane, K.T. Carron, Anal. Chem. 64 (1992) 930.
[32] G.L. Bertrand, Discussion on the Surface pH, personal communication, 1993.
[33] J. Sonnefeld, J. Colloid Interface Sci. 155 (1993) 191.
[34] D. Mobius, W. Cordroch, R. Loschek, L.F. Chi, A. Dathathreyan, V. Vogel, Thin Solid Films 178 (1989) 53.
[35] J. Albery, Electrode Kinetics (Oxford Chemistry Series), Clarendon Press, Oxford, 1975.